communications biology

Article

https://doi.org/10.1038/s42003-024-07056-x

Insights into the molecular characteristics of embryonic cranial neural crest cells and their derived mesenchymal cell pools

Hengxing Ba[1,4] ✉, Qianqian Guo[1,4], Yudong Shang[1], Pengfei Hu[1], Chao Ma[1], Jiping Li[1], Dawn Elizabeth Coates[2] ✉ & Chunyi Li[1,3] ✉

Neural crest cells (NCCs) are central to vertebrate embryonic development, giving rise to diverse cell types with unique migratory and differentiation capacities. This study examines the molecular characteristics of cranial neural crest cell (CNCC)-derived mesenchymal cells, specifically those from teeth which in deer show continuous but limited growth, and antlers, which exhibit remarkable regenerative capabilities. Here, through single-cell RNA sequencing analysis, we uncover shared gene expression profiles between adult antlerogenic and dental mesenchymal cells, indicating common developmental pathways. We identify a striking resemblance in transcriptomic features between antlerogenic progenitor cells and dental pulp mesenchymal cells. Comparative analysis of CNCC-derived and non-CNCC-derived mesenchymal cell pools across species reveals core signature genes associated with CNCCs and their derivatives, delineating essential connections between CNCCs and CNCC-derived adult mesenchymal pools. Furthermore, whole-genome DNA methylation analysis unveils hypomethylation of CNCC derivate signature genes in regenerative antlerogenic periosteum, implying a role in maintaining multipotency. These findings offer crucial insights into the developmental biology and regenerative potential of CNCC-derived mesenchymal cells, laying a foundation for innovative therapeutic strategies in tissue regeneration.

Neural crest cells (NCCs) are found only in vertebrates. They are a multipotent developmental population present during gastrulation with unique long-range migratory potential and differentiation capacity. Some consider NCCs to be ectoderm as they transiently resided in the dorsal neural tube before delaminating and migrating; their unique characteristics have also led others to identify them as the fourth germ cell layer[1–3]. The neural crest is segmented into cranial, vagal, trunk, and sacral regions controlled by a neural crest gene regulatory network (GRN), with each segment having site-specific regulatory influences. The focus of this research is the cranial NCCs (CNCCs), which contribute to the head and superior neck derivates[4] and retain a unique pluripotency signature producing derivates of ectoderm and mesoderm[5,6].

Distinct populations of cells form during the migration of CNCCs controlled by both the local environment and the GRN, which then result in odontoblasts, osteoblasts, smooth muscle cells, adipocytes, melanocytes, neurons, Schwann cells, chondroblasts, thymic cells, cornea, thyroid and connective tissues cells[7,8]. CNCC-derived mesenchymal pools are retained in different adult tissues. High-density repositories of multipotent CNCC derivates suitable for regenerative medicine can be found in teeth pulp, apical papilla, periodontal ligament, and the periosteum of craniofacial bone. Three pools of dental-related mesenchymal cells (MCs) are of particular interest: the tooth bud dental mesenchymal cells (DeMCs) responsible for the development of a tooth in the embryo, dental pulp mesenchymal cells (DPMCs) from human exfoliated deciduous teeth pulp and adult dental pulp. When comparing human and deer DPMCs it should be noted that, unlike humans, deer adult molars have some limited growth by cementocytes producing secondary cementum, and this process is likely driven by MCs[9]. The ability of human DPMCs to differentiate into adipocytes, chondroblasts, and osteoblasts is well documented, along with skeletal muscle[10] and cardiomyocyte[11] derivatives.

In the animal kingdom, deer antlers are undoubtedly the most remarkable example of CNCC-derived regeneration, where the antler has a

[1]Jilin Provincial Key Laboratory of Deer Antler Biology, Institute of Antler Science and Product Technology, Changchun Sci-Tech University, 130600 Changchun, China. [2]Sir John Walsh Research Institute, Faculty of Dentistry, University of Otago, Dunedin, New Zealand. [3]College of Chinese Medicinal Materials, Jilin Agricultural University, Changchun, 130118, China. [4]These authors contributed equally: Hengxing Ba, Qianqian Guo. ✉e-mail: bahengxing@cstu.edu.cn; dawn.coates@otago.ac.nz; lichunyi1959@163.com

complex adult structure, regenerating annually at up to 2 cm/day. Antler is an example of microevolutionary diversity driven by CNCCs[12]. Within the antlerogenic periosteum (AP) on deer frontal bone is a pool of AP mesenchymal cells (APMCs), which later differentiate into AP progenitor cells (APPCs)[13]. When triggered, these cells give rise to a short pedicle, followed by the growth of the first antler. In subsequent years, the antler develops from the pedicle, with a pool of subdermal mesenchymal cells at the antler tip responsible for its growth. In a similar way to DPMCs, in vitro studies have shown that APMCs possess the capacity to differentiate into multiple lineages including adipocytes, chondroblasts, and osteoblasts[14,15].

Enhancing our understanding of the relationship between embryonic CNCCs and various derivative multipotent CNCC-derived mesenchymal pools holds significant promise for advancing our knowledge of the GRN, regenerative control mechanisms, differentiation potential, therapeutic applications, and characteristic attributes of CNCCs. Most studies investigating CNCC-derived mesenchymal cells in adult tissues have focused on characterizing resident cells based on CNCC markers, lineage mapping, or the differentiation capacity of these cells. Current technological limitations have hindered comprehensive gene assessment of adult multipotent CNCC-derived mesenchymal pools. Furthermore, no research to date has explored the interconnections among diverse adult mesenchymal pools through single-cell RNA sequencing (scRNA-seq). This investigation aims to bridge this gap by conducting cross-species scRNA-seq analysis on CNCC-derived mesenchymal pools obtained from antler and teeth tissues, shedding light on their molecular characteristics and potential applications.

DNA methylation, a highly conserved epigenetic modification found in most plant and animal models[16], has a profound impact on genome stability and gene expression[17,18]. During development, epigenetic repression via DNA methylation is a prevalent mechanism for shutting down alternative pathways during cell type specification and lineage commitment[19]. Moreover, DNA methylation is a critical regulator in neural crest specification, migration, and differentiation[20]. Disruption of DNA methylation-mediated cranial neural crest proliferation and differentiation leads to orofacial clefts in mice[21]. AP tissue demonstrates remarkable regenerative abilities during initial deer antler development. However, adjacent tissues like facial periosteum (FP) tissue from deer, which also originate from CNCC, lack such regenerative capabilities. In this study, we conducted whole-genome DNA methylation analysis to compare the DNA methylation profiles of these two types of periosteum tissues, specifically examining changes in DNA methylation levels of CNCC derivate signature genes. This research conducted single-cell sequencing on deer molar pulp and genome bisulfite sequencing on AP. It compared these with existing databases of CNCCs (mouse) and derivative pools of AP, deer FP, and teeth (deer/human/mouse).

We hypothesize that single cell sequencing will detect a pool of cells in embryonic CNCC cells with similarities to regenerative pools retained in both the AP and tooth mesenchyme/pulp which display high regenerative capacity; we also propose that hypomethylation will be an important regulatory mechanism in deer AP cells.

Results

Adult deer APMCs and DPMCs express CNCC derivate signature genes

The identification and characterization of CNCC derivate signature genes expressed in APMCs and DPMCs represent a significant advancement in understanding the regenerative potential of these tissues. A cross-species approach was adopted due to the challenges associated with obtaining unmodified deer CNCCs. Wnt1-traced CNCCs were obtained from previously published studies[22] conducted on the mouse anterior half of embryos at the E8.5 developmental stage (Fig. 1A). Cross-species integration of the scRNA-seq data from deer AP, deer molar dental pulp tissue, and mouse Wnt1-traced E8.5 CNCCs (Fig. 1B), enabled us to perform unsupervised clustering analysis. Using known gene markers, we identified key cell populations (Fig. 1C, D, Supplementary Fig. 1A, B), with a particular focus on mouse *SOX2*$^+$ neural tube cells, *SOX10*$^+$ migrating CNCCs, and *TWIST1*$^+$ mesenchymal CNCCs[22], and deer *THY1*$^+$ APMCs, *TNC*$^+$ APPCs[13], deer *MSX2*$^+$ DPMCs[23–25]. Very few *WNT1*$^+$ NT signature genes (*WNT1*, *SOX2*, *HES5*) or neural plate border signature genes (*PAX3*, *PAX7*, *ZIC1*, *ZIC3*, *TFAP2A*) were found in APMCs and DPMCs. Upon further investigation of known signature genes related to EMT/migrating CNCCs[3,26,27], we found that deer APMCs and DPMCs exhibited significant expression levels of EMT/migrating CNCC signature genes *MYC*, *ZEB2*, *ID3*, *CDH2*, *SOX9*, *MAFB*, *ID4*, *ETS1*, *EBF1*, *SNAI1* and *CDH1* but with only low/no expression *FOXD3* or *SOX10* (Fig. 1E). When considering the signature genes related to migrating/mesenchymal CNCCs, deer DPMCs highly expressed *DLX2*, and both DPMCs and APMCs expressed *MSX2*, *TWST1*, and *PRRX2*. Cranial ectomesenchyme signature genes *SNAI2*, *PRRX1*, and *TWIST2*, were highly expressed in both deer APMCs and DPMCs. The retention of particularly the EMT/migrating CNCC derivate signature genes in adult antler and teeth tissue points to critical factors that could be important for the activation of growth and repair post-embryonic development.

The transcriptional features of APMCs differentiating into APPCs closely resemble those observed during DeMCs differentiation from mouse embryonic to postnatal stages

We investigated whether different CNNC-derived resident MC populations have similar transcriptional signatures as they differentiate. To do this, we examined whether deer antler APMCs differentiating into APPCs share similar transcriptional molecular characteristics and undergo analogous early differentiation processes as observed during tooth development. We utilized published scRNA-seq datasets from embryonic and early postnatal mouse molar tissues at various developmental stages[25], including E13.5, E14.5, E16.5, P3.5, and P7.5. After integrating these datasets, we performed an unsupervised clustering analysis (Supplementary Fig. 2A). Cells were then assigned to 21 clusters, with two clusters (C0 and C1) identified as DeMCs (Fig. 2A, B, Supplementary Fig. 2B, C). Notably, these two clusters exhibited distinct distribution patterns: C0 was predominantly present during the E13.5, E14.5, and E16.5 stages, while C1 was primarily observed during the P3.5 and P7.5 stages (Fig. 2B and Supplementary Fig. 2D), suggesting a trajectory from C0 to C1 as DeMCs transition from tooth germ stages to postnatal stages. We utilized the scPred tool to compare the transcriptional profiling of APMCs and APPCs as references to those of mouse DeMCs at various developmental stages (Fig. 2C, D). When restricted to these two cell types (APMCs and APPCs), our scPred analysis revealed that DeMCs during the E13.5 and E14.5 stages exhibited nearly identical similarity to APMCs, with an average probability exceeding 98% (Fig. 2E, F). Furthermore, from the E16.5 to P7.5 stages, 77% of DeMCs showed similarity (probability > 75%) to APMCs, while 18% of DeMCs displayed similarity to APPCs (Fig. 2G, H).

The earliest initiators of antler development are APMCs, which later differentiate into APPCs expressing specific signature genes, including *DLX5*, *RUNX2*, *TNC*, and *PTN*[13]. We investigated whether these signature genes of APPCs are also expressed during DeMCs early differentiation. To investigate this, we compared the expression levels of these genes during DeMCs differentiation, alongside CNCC signature genes such as *MSX1*, *MYC*, *ZEB2*, *ID3*, *SOX9*, *MAFB*, *ID4*, *EBF1*, *SNAI1*, *MSX2*, *TWIST1*, and *PRRX2*. The results revealed highly similar expression patterns for these genes during both antler and tooth development processes (Fig. 2I). These findings suggest that CNCC-derived mesenchymal cells show similarities in gene expression, but can subsequently differentiate into specialized tissues such as antlers and teeth.

We further conducted a consensus co-expression network to identify gene modules in deer APMCs, APPCs, and mouse DeMCs (Fig. 3A). A total of 17 co-expression modules resulted from the network analysis (Fig. 3B). Two co-expression gene modules, named M1 and M2, displayed high harmonized module eigengenes (hMEs; Fig. 3C). Module M1 was shared between APMCs and DeMCs (C0) during the early tooth germ stage, while M2 was shared between APPCs and DeMCs (C1) during the postnatal germ stages. The hub genes within M1 are associated with the regulation of cell

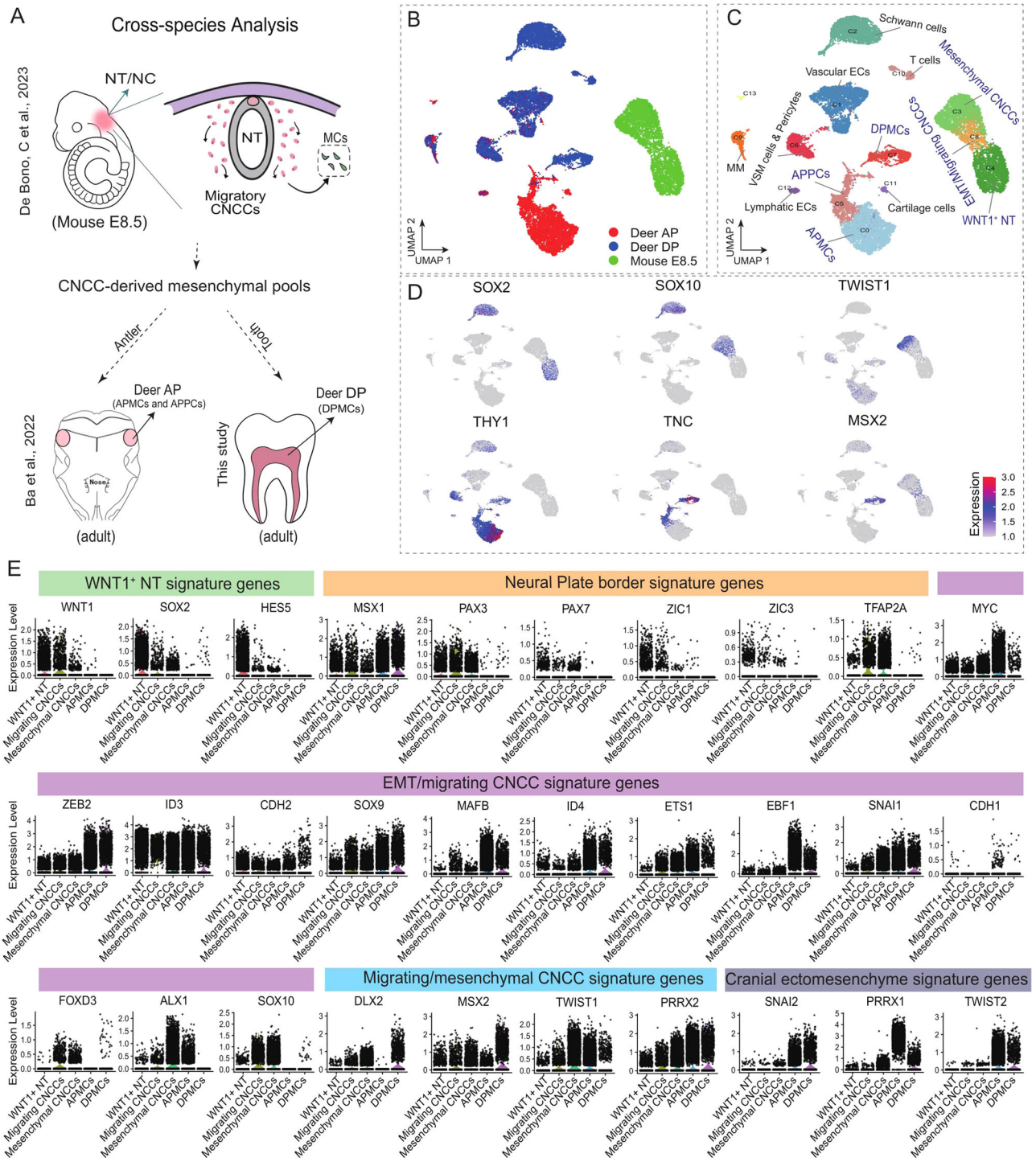

Fig. 1 | Cross-species single-cell profiling of both CNCC-derived organs: antlers and teeth. A Schematic location of mouse E8.5 Wnt1-traced neural tube (NT)/neural crest (NC) with scRNA-seq data obtained from[22], deer antlerogenic periosteum (AP) and deer teeth dental pulp (DP) mesenchymal cells (DPMCs). Note that prior to NT closure, epithelial-to-mesenchymal transition (EMT) triggers CNCCs to delaminate from the NT and migrate throughout the embryo to locate in different cranial regions. CNCCs possess diverse differentiation potentials, highlighting their capability to give rise to mesenchymal cells (MCs). Within the deer AP on the frontal bone locates a pool of AP mesenchymal cells (APMCs), which later differentiate into APPCs[13]. Both APMCs and DPMCs are CNCC-derived. **B** UMAP plot to visualize all cells from the mouse CNCCs, deer AP, and DP; tissue types are color-coded. **C** UMAP plot to visualize the unsupervised clusters along with the cell types identified from the mouse E8.5 CNCCs, deer AP, and DP. The cell types with a particular focus are labeled in blue. **D** UMAP plot to visualize the expression levels of marker genes associated with CNCC development. *WNT1*$^{+}$ NT (SOX2), EMT/migrating CNCCs (*SOX10*), migrating/mesenchymal CNCCs (*TWIST1*), APMCs (*THY1*), APPCs (*TNC*), and DPMC (*MSX2*). **E** Violin plots to illustrate the expression of signature genes associated with various stages of *WNT1*$^{+}$ NT, Neural Plate border, EMT/migrating CNCCs, migrating/mesenchymal CNCCs, and cranial ectomesenchyme within the populations of *WNT1*$^{+}$ NT, EMT/migrating CNCCs, mesenchymal CNCCs, APMCs, and APPCs.

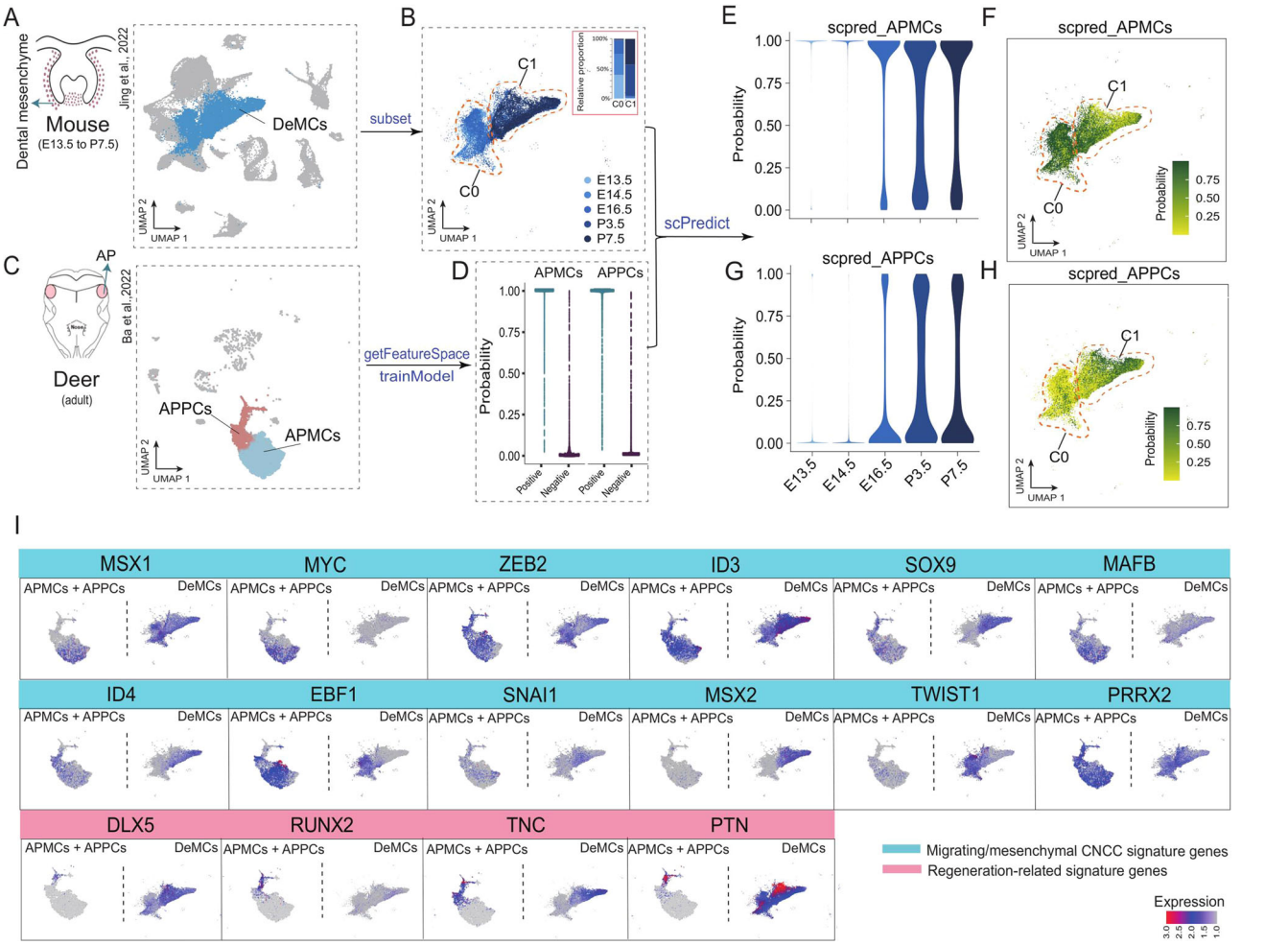

Fig. 2 | Shared transcriptional features of deer APMCs + APPCs and mouse DeMCs during their initial differentiation. A Schematic drawing of mouse tooth molar tissues at various developmental stages, including tooth germ stages E13.5, E14.5, and E16.5, as well as postnatal stages P3.5 and P7.5 with scRNA-seq data obtained from[26] in a UMAP plot displaying DeMCs. **B** UMAP plot to visualize DeMCs, consisting of two clusters (C0 and C1). The red box highlights the relative proportion of these two clusters at various developmental stages. **C** Schematic drawing of AP tissues, along with a UMAP plot to visualize APMCs and APPCs. **D** Dot plots to show training probabilities for each cell of both APMCs and APPCs based on the scPRed tool. **E** Violin plots to illustrate the predictive probabilities of APMCs for each cell in the mouse DeMCs at various developmental stages. **F** UMAP plot to visualize the predictive probabilities of APMCs for each cell in the mouse DeMCs at two clusters (C0 and C1). **G** Violin plots to illustrate the predictive probabilities of APPCs for each cell in the mouse DeMCs at various developmental stages. **H** UMAP plot to visualize the predictive probabilities of APPCs for each cell in the mouse DeMCs at two clusters (C0 and C1). **I** UMAP plot to visualize co-expression patterns of 12 CNCC signature genes and 4 regeneration-related signature genes in APMCs + APPCs and mouse DeMCs.

differentiation, cell development, and neurogenesis (Fig. 3D), regulated by key hub genes, including *IGF2*, *SFRP2*, *FOXP2* and *NEGR1* (Fig. 3E). Moreover, the hub genes in M2, such as *MSX2*, *TNC*, *ALPL*, *OMD*, *PTCH1*, and *DLX3*, are related to animal organ morphogenesis, ossification, biomineral tissue development, and odontogenesis (Fig. 3D). This is the first time the core genes linked to CNCC-derived adult mesenchymal pools have been identified across diverse organs.

APPCs exhibit a molecular characteristic remarkably similar to that of adolescent human DPMCs

To enhance our understanding of the molecular characteristics of the CNCC-derived craniofacial GRN in adult tissues, we conducted a cross-species integrated scRNA-seq analysis between deer AP and dental pulp samples from adult deer and adult and adolescent humans (Fig. 4A). The abundance of MCs in the adult dental pulp and growing apical papilla is well-established. Their scRNA-seq data were collected in a separate study[23]. Unsupervised clustering analysis unveiled 19 distinct clusters (Fig. 4B, C). Among these clusters, C2 and C6 were primarily composed of *THY1*$^{+}$ APMCs, which are predominantly found in the AP. Additionally, six clusters (C1, C4, C7, C11, C14, and C19) exhibited high expression of marker genes specific to both APPCs (e.g., *TNC*) and DPMCs (e.g., *MSX2*) (Fig. 4D), indicating that these clusters were shared between APPCs and DPMCs. Specifically, APPCs were predominantly located within three clusters (C1, C4, and C14), while DPMCs were primarily distributed across these six clusters (Fig. 4E). Furthermore, we identified eight distinct cell types within these tissues (Supplementary Fig. 3A–C), including vascular smooth muscle cells and pericytes (C5), vascular endothelial cells (C0, C8, C12, and C17), lymphatic endothelial cells (C18), monocytes/macrophages (C9), odontoblasts (C16), Schwann cells (C3), glial cells (C13), and T cells (C10). Particularly noteworthy was the identification of a population of proliferative cells (C15). Within the APPCs + DPMCs group, it was observed that the percentage of DPMCs was significantly higher in adolescent human apical papilla tissue compared to the other tissues (Fig. 4F), thus potentially indicating the loss of regenerative potential in human teeth with aging. Conversely, human adult dental pulp exhibited only minimal proliferative cells and a predominance of odontoblasts (Supplementary Fig. 3D). Interestingly, the absence of gene expression specific to signature genes of CNCC derivates, such as *SOX9*, *SNAI2*, *HAPLN1*, and *TWIST2* (Fig. 4G), in adult human DPMCs suggested a higher level of cellular differentiation with aging.

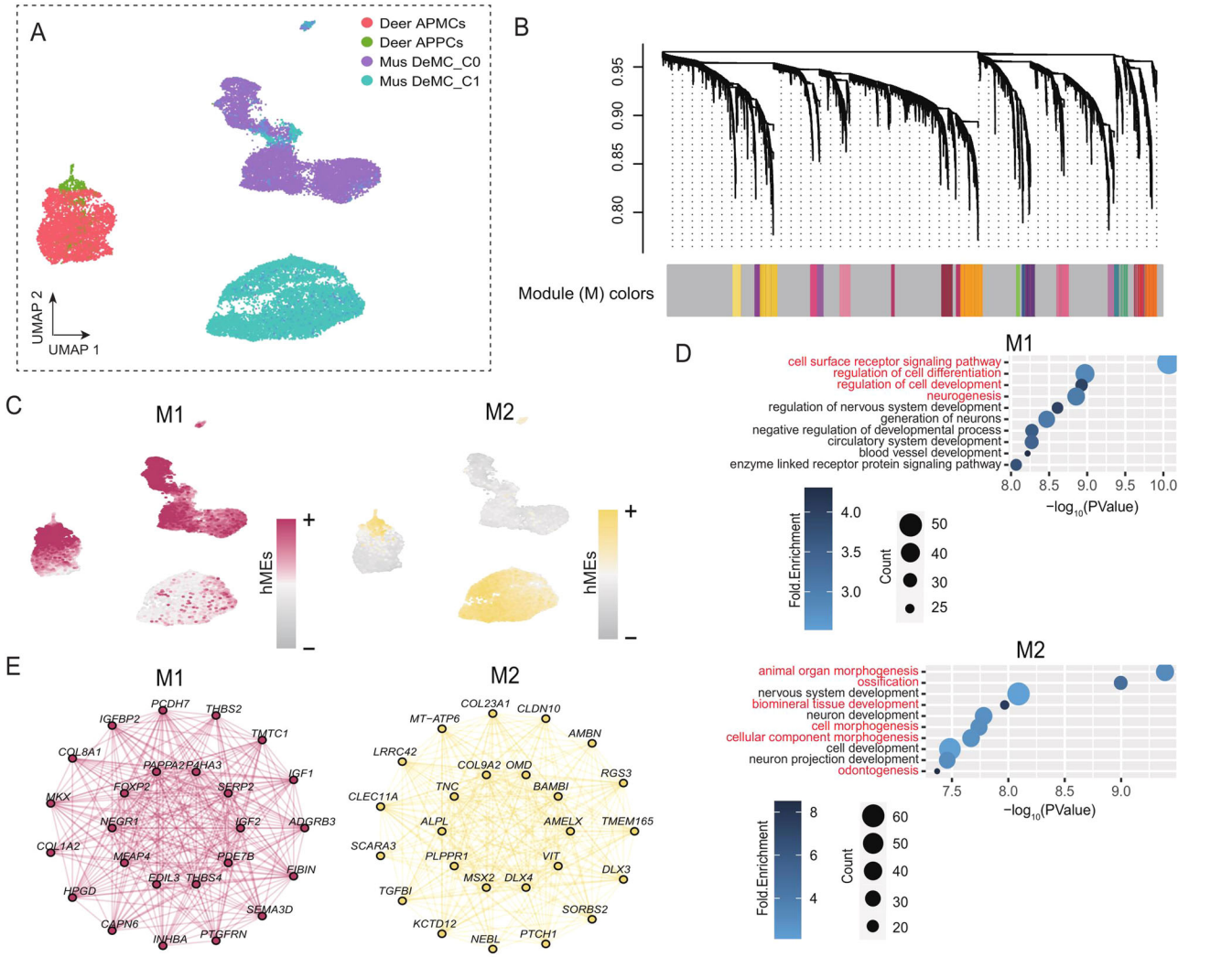

Fig. 3 | Co-expressed consensus networks of APMCs, APPCs, and mouse DeMCs. **A** UMAP plot is visualizing APMCs, APPCs, mouse DeMCs (C0), and DeMCs (C1). **B** hdWGCNA dendrogram illustrating the different co-expression modules that resulted from the network analysis. Each leaf on the dendrogram denotes a single gene, and the color, except for gray, at the bottom, indicates the co-expression module assignment. The gray modules comprise genes that were not assigned to any specific co-expression module. **C** UMAP plot to visualize the hMEs for the modules of M1 and M2. Note that M1 showed high hMEs between APMCs and mouse DeMCs (C0), and M2 showed high hMEs between APPCs and mouse DeMCs (C1). **D** Networks underlying the top 25 hub genes for the M1 and M2 modules, respectively. Each node denotes a gene, and each edge denotes the co-expression relationship between two genes in the network. **E** Dot plot to show the DAVID enriched Gene Ontology BP terms (top 10) using all hub genes in the modules of M1 and M2, respectively.

Over 80% of the highly expressed genes in the APPCs + DPMCs group were associated with ossification, animal organ morphogenesis, and stem cell differentiation (Fig. 4H). The top 50 highly expressed genes included signature genes of CNCCs derivates (e.g., *HAPLN1* and *MSX1*), DPMCs (e.g., *MSX2*), and APPCs (e.g., *DLX5*, *PTN*, and *TNC*) (Fig. 4I). These genes are implicated in bone and neuron development, emphasizing the intricate coordination between CNCC-derived APPCs and DPMCs during development. Additionally, we pinpointed highly expressed genes specific to APPCs and each of the DPMCs in humans and deer. Our analysis revealed 35 genes that consistently exhibited high expression levels across these four samples (Fig. 4J). Notably, 75% of these genes were among the top 50 highly expressed genes in the APPCs + DPMCs group, and these genes were also consistently involved in functional enrichment results (Supplementary Fig. 3E), further indicating similar molecular characteristics between APPCs and DPMCs. Among these 35 co-expressed genes, five genes have previously been associated with pluripotent stem cells: *PTN*, *GJA1*, *DLX5*, *NES*, and *FN1* (Fig. 4K). A STRING-db network also found *SATB2*, *NOTCH2*, *ROBO1*, *FAT3*, *CDH11*, and *DKK3*, associated with these five stem cell regulators (Fig. 4L). These genes may thus identify an interconnected network for the identification of post-embryonic CNCC-derived mesenchymal pools.

The global transcriptomic signatures of APPCs more closely resemble that of deer DPMCs than that of human DPMCs

The global transcriptional similarity among these four cell populations (APPCs and each of the DPMCs in humans and deer) can provide insights into the evolutionary developmental relationships between them. To do so, we conducted a comprehensive comparison of their transcriptomes. The results revealed an intriguing pattern: there was a stronger correlation between APPCs and deer DPMCs compared to human DPMCs (Fig. 4M). Thus, the dental pulp cells from different species have evolved to have distinct transcriptomic signatures. This observation suggests that APPCs and deer DPMCs may share similar developmental pathways and regulatory mechanisms that distinguish them from human DPMCs, and this may be linked to the species-specific evolution of the CNCCs. To further investigate their shared regulatory mechanisms, we employed a SCENIC workflow to identify cell-type regulons, which are co-expressed transcription factors and their putative target genes in the regulatory network, that

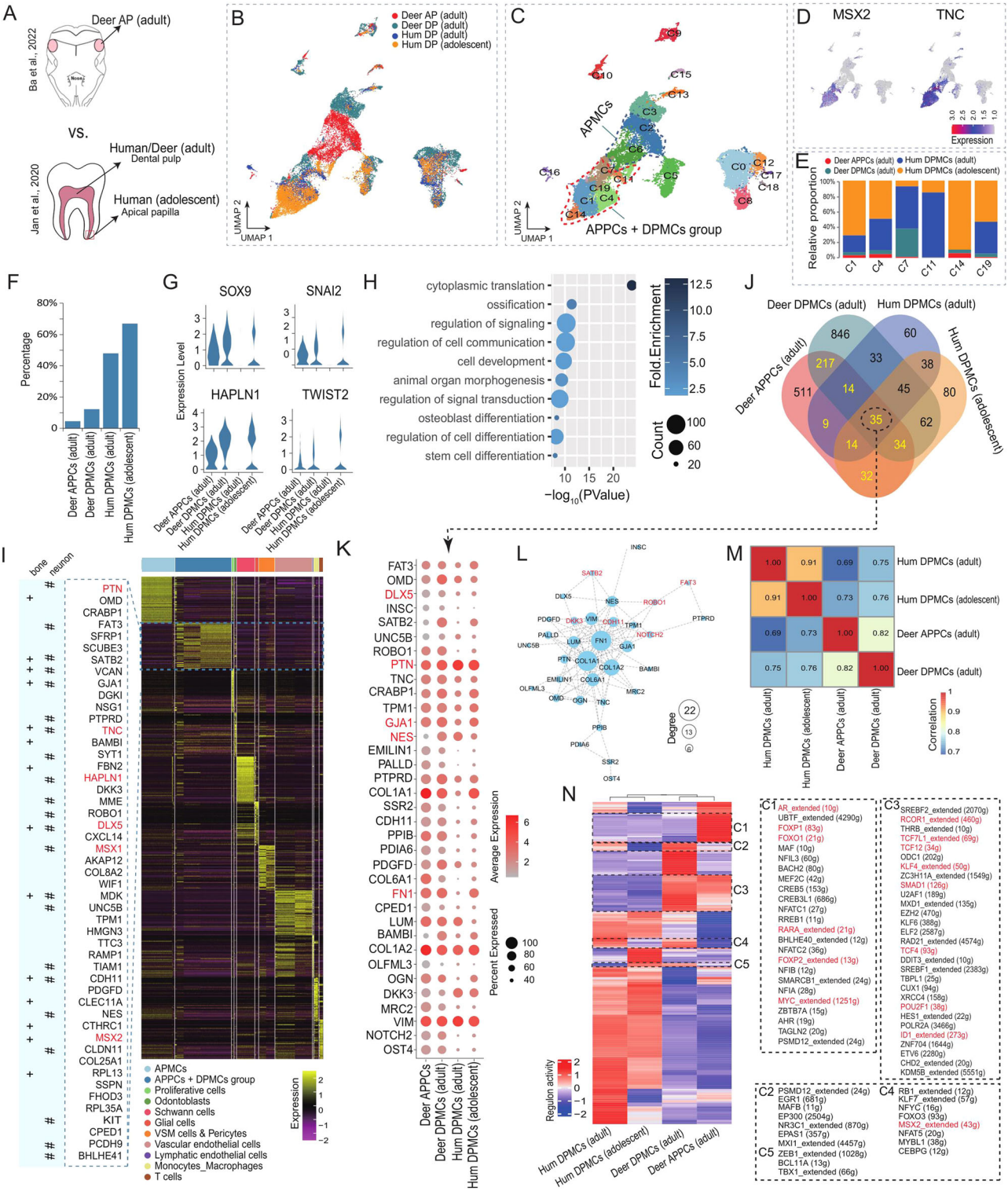

play key roles in controlling cell fate specification and differentiation. The hierarchical clustering based on regulon activity also indicated stronger correlations between APPCs and deer DPMCs (Fig. 4N). The analysis unveiled a specific regulon cluster (C1) in APPCs, which included transcription factors such as *AR*, *MYC*, *RARA*, and *FOXO1*. These transcription factors are known to play important roles during antler development[1314,28–32]. A substantial cluster (C3) comprising 29 shared regulons was identified between APPCs and deer DPMCs. Within these regulons, several transcription factors are known for their roles in stem cell maintenance, embryonic development, and organ/tissue development, including *RCOR1*, *KLF4*, *POU2F1*, *SMAD1*, and *ID1*. Additionally, the presence of the TCF superfamily, including *TCF12*, *TCF4*, and *TCF7L1*, in both APPCs and deer DPMCs aligns with their established importance in the development of craniofacial structures derived from CNCCs[33]. Three clusters (C2, C4, and C5) are co-activated in both deer and adult or adolescent human DPMCs, comprising a total of 19 regulons, suggesting that these regulons may play a role in tooth development, with an example being *MSX2*. Altogether, these findings provide valuable insights into the shared molecular mechanisms

Fig. 4 | Integrated single-cell analysis of APPCs and adult human and deer DPMCs. A Schematic illustration of deer AP, adolescent and adult human, and adult deer dental pulps. Human scRNA-seq data obtained from[23]. **B** UMAP plot to visualize all cells from AP and dental pulps, tissue types are color-coded. **C** UMAP plot to visualize unsupervised clusters along with the identification of APMCs and APPCs in AP and DPMCs in dental pulps. **D** UMAP plot to visualize the expression of marker genes within the APPCs + DPMCs group, including *MSX2* and *TNC*. **E** Bar plot to show the relative proportions of unsupervised clusters within the APPCs + DPMCs group. **F** Bar graph with the percentage of APPCs and DPMCs. **G** Violin plots to illustrate the expression of CNCC derivate signature genes within the APPCs + DPMCs group. **H** Dot plot to show DAVID enriched Gene Ontology terms using highly expressed genes within the APPCs + DPMCs group. **I** Heat map plot to illustrate the expression profiles of the top 50 highly expressed genes in all cell types. The left side of the heat map lists the top 50 highly expressed genes within the APPCs + DPMCs group. The genes related to bone (*) and neuron (#) development are also marked. The signature genes related to CNCCs derivates (e.g., *HAPLN1* and *MSX1*), DPMCs (e.g., *MSX2*), and APPCs (e.g., *DLX5*, *PTN*, and *TNC*) are highlighted in red. J. Venn plot to show highly expressed genes specific to APPCs and each of the human and deer DPMCs. **K** Dot plot to show 35 shared genes in (**J**) that are related to bone and neuron development. The size of each dot represents the percentage of cells expressing the gene, while the shade of color represents the average expression level of the gene. The genes (e.g., *PTN*, *GJA1*, *DLX5*, *NES*, and *FN1*) related to pluripotent stem cells are highlighted in red. **L** STRING-db network of the 35 shared genes in (**J**). Nodes represent genes. The size of the node indicates the degree of connection; the larger the node, the higher the degree of connection with others for a given gene. The genes relevant to the context of the study are highlighted in red. **M** Heat map plot to illustrate correlations between cell types within the APPCs + DPMCs group, calculated based on average expressed scRNA-seq data. Pearson correlation coefficients are shown. **N** Heat map plot to illustrate the activity of regulons between cell types within the APPCs + DPMCs group. Five specific regulon clusters are highlighted by a black dashed box. The right side of the heat map lists the active regulons in these five regulon clusters. The regulons highly relevant to the context of the study are highlighted in red.

underlying the CNCC-derived development of antlers and teeth in deer, shedding light on similar regulatory networks and key transcription factors.

Molecular characteristic of CNCC-derived mesenchymal cell pools during embryonic and postnatal stages across humans, mice and deer

To more fully characterize CNCC-derived MC pools, we expand our analysis to encompass various scRNA-seq data across humans, mice, and deer in both embryonic and postnatal stages (Fig. 5A), including the mouse migrating/mesenchymal CNCCs[22], deer APMCs and APPCs, deer CNCC-derived FP mesenchymal cells (FPMCs) and FP progenitor cells (FPPCs)[13] and molar DPMCs from sika deer, tusk and molar DPMCs from Chinese water deer (CWD), a unique deer species characterized by the absence of antlers but possessing a set of large tusks, mouse DeMCs of tooth germ and postnatal stages[25], as well as human DeMCs of tooth germ (Supplementary Fig. 4A–C)[24] and adolescent and adult DPMCs[23]. Additionally, 11 types of non-CNCC-derived MCs from 11 human fetal organs[34] were included in the analysis.

After isolating annotated MC types from these data sources and normalizing the data, we assessed the expression of 35 signature genes among these MC pools. The key findings are summarized as follows (Fig. 5B): (1) CNCC-derived MCs exhibited significantly higher expression of these signature genes compared to non-cranial counterparts; (2) *WNT1*$^{+}$ neural tube signature genes (*WNT1*, *SOX2*, *HES5*) along with EMT/migrating CNCC genes *FOXD3*, *SOX10* and possibly *ZIC3* (low expression only) were restricted to mouse embryonic CNCCs; (3) *MSX1*, *ID3*, *CDH2*, *SOX9*, *MAFB*, *ID4*, *ETS1*, *SNAI1*, *TWIST1*, and *PRRX2* form a marker gene set for embryonic CNCCs and CNCC-derived MCs; (4) *DLX2* and *MSX2* were identified as signature genes for teeth DeMCs/DPMCs and embryonic CNCCs (but not other CNCC-derived tissues). Interestingly, *TFAP2A* was strongly expressed in embryonic CNCCs, and CWD tusk DPMCs with weak expression in human embryonic DeMCs; (5) cranial ectomesenchyme-related signature genes and regeneration-related genes *SNAI2*, *TWIST2*, *RUNX2*, and *TNC* showed high expression specifically in CNCC-derived MCs; (6) *ZEB2*, *EBF1*, *PRRX1*, and *PTN* where found to have a more generic expression across both cranial and non-cranial MCs. These findings provide valuable insights into the origin and molecular characteristics of CNCC-derived and non-CNCC-derived MC pools from diverse tissues and organs, spanning embryonic and postnatal stages across different species, and emphasize their inherent properties. These gene signatures add to existing knowledge of identifying different CNCCs and derivative pools along with the core genes that can detect both CNCCs and their derivative pool: *MSX1*, *ID3*, *CDH2*, *SOX9*, *MAFB*, *ID4*, *ETS1*, *SNAI1*, *TWIST1*, and *PRRX2*.

DNA hypomethylation of CCNC derivate signature genes was maintained in the AP compared to the FP

Epigenetic regulation via DNA methylation plays a crucial role in neural crest specification, migration, and differentiation[20]. To elucidate the intrinsic regulatory mechanisms governing the maintenance of multipotency in CNCC-derived MCs, we utilized AP as a representative example of CNCC derivatives. We conducted whole-genome bisulfite sequencing analysis on deer AP and FP tissues as controls (Supplementary Fig. 5A, B). Our analysis revealed that 66.3–72.9% of cytosines in CpG sites across the entire genome were methylated, whereas less than 1% of cytosines in CHG and CHH contexts were methylated (Supplementary Fig. 5C). Specifically focusing on CpG site methylation, we observed that hypomethylated CpG sites were predominantly situated near the transcription start site (TSS) (Fig. 6A). Notably, hypomethylation levels in the promoter region of the AP (11% based on |diff. Methy| > 0.3 and 23% based on |diff. Methy| > 0.1) were higher compared to those in the FP (2% and 2%) (Fig. 6B and Supplementary Data 1).

Through a comprehensive analysis associating genomic regions with genes in a many-to-many mapping scheme, covering gene bodies, promoters (±1000 bp), and adjacent intergenic regions (3000 bp), we identified 932 hypomethylated and 642 hypermethylated genes in the AP compared to the FP. These genes primarily participate in neuron migration and developmental processes (Fig. 6C). Furthermore, we uncovered an association between hypomethylation and CNCC derivate signature genes including *MSX1*, *TFAP2A* and *PAX3* as well as cranial ectomesenchyme signature gene *TWIST2* in the AP (Fig. 6D and Supplementary Fig. 5E). Hypomethylated CpG sites were found within and near these genes, particularly in close proximity to their promoters. Remarkably, no hypermethylated CNCC signature genes were identified. The AP cells have previously been reported to form colonies, express stem cell markers, produce chimera in vivo, and exhibit multi-lineage differentiation capacity[15]. Thus, findings suggest that epigenetic regulation via DNA hypomethylation of promoter regions may contribute to the maintenance of multipotency in the AP, underscoring the importance of DNA methylation status in preserving multipotency in adult CNCC-derived MCs, future research should be conducted to confirm this.

Discussion

DeMCs during early-stage tooth bud mouse embryo (E13.3–14.5) and APMCs were found to be 98% similar based on their transcriptional profiling comparison (Fig. 2E). This finding suggests that these two distinct CNCC-derived tissues have pools of cells with similarities, and warrants further research on their relationship with nascent CNCC's. APPCs have been shown to express specific signature genes, including *DLX5*, *SOX9*, *RUNX2*, *TNC*, and *PTN*[13]. These genes are also associated with PDGFRA-expressing MCs[35,36] driving regenerating digit tips in mice[37]. Hence, we termed these genes as "regenerated signature genes". Interestingly, these genes were found to be highly expressed in post-natal 3.5/7.5 stage DeMCs as well (Fig. 2I). These results indicate that despite residing in different mesenchymal pools and regardless of their location, there is consistency in the expression of these regenerated signature genes. Two key co-expressed

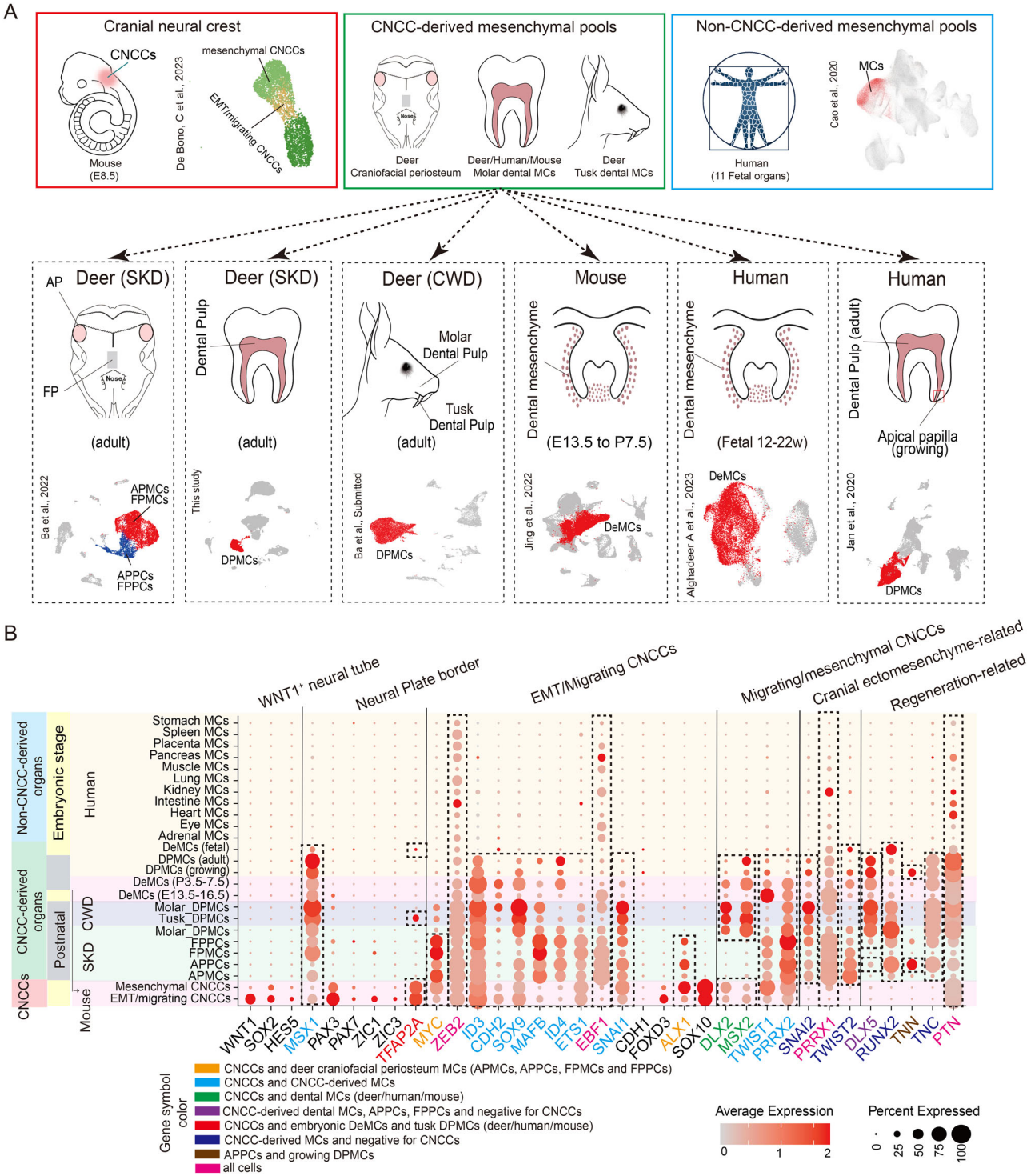

Fig. 5 | Expression pattern analysis of the 32 key signature genes for CNCC-derived mesenchymal pools during embryonic and postnatal stages across human, mouse, and deer. A Schematic location and UMAP plot of CNCC-derived mesenchymal pools: deer craniofacial periosteum cells, including APMCs, APPCs, FPMCs, and FPPCs[13], adult deer dental pulps (this study), CWD tusk and molar dental pulps, human tooth germ tissues at 12–22[24] weeks, human dental pulps, including both adult and growing tooth (Jan et al., 2020), mouse dental pulp at various developmental stages, including tooth germ stages E13.5, E14.5, and E16.5, as well as postnatal stages P3.5 and P7.5[26]. Non-CNCC-derived mesenchymal pools: 11 human fetal organs[35]. **B** Dot plot to show 35 key signature genes associated with CNCC derivates and CNCC-derived mesenchymal pools. Note that 35 key signature genes were further classified based on their expression pattern across these samples, classification are color-coded.

modules (M1 and M2) link antler development and tooth bud induction, representing the first report of such gene co-expression modules. This further highlights the transcriptional features of APMCs differentiating into APPCs that closely resemble those observed during DeMCs differentiation from mouse embryonic to postnatal stages.

Antler regeneration involves the depletion of a pool of MCs that initiate endochondral bone formation, resulting in a structure weighing 0.5–8 kg

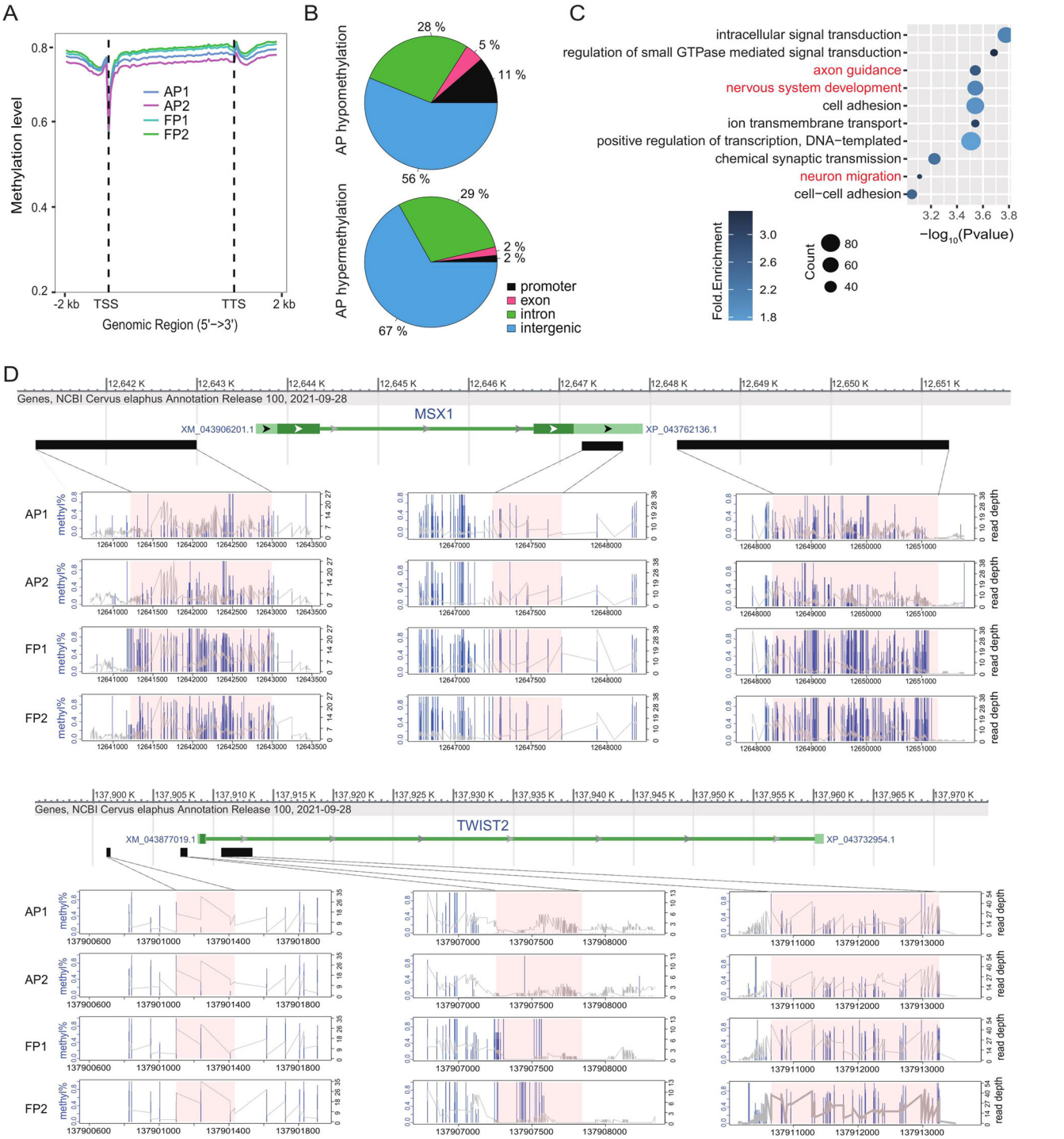

Fig. 6 | Whole-genome bisulfite sequencing reveals hypomethylation of CNCC derivate signature genes in the AP tissue. A Distribution of methylation level in the AP and FP with two replicates: TSS transcriptional start site and TTS transcriptional terminal site. **B** Pie chart to show the percentage of hypermethylation and hypomethylation based on |diff. Methy| > 0.3 in different genetic regions (promoter, exon, intron, intergenic) in AP vs. FP. Promoters for each gene are limited to ±1000 bp around the TSS. Note the high proportion of hypomethylation in the promoter region in AP. **C** Dot plot to show DAVID enriched Gene Ontology terms using the genes associated with differentially methylated regions. **D** Hypomethylated regions (indicated by black bars) in AP vs. FP are located within or around CNCC derivate signature genes *MSX1* and *TWIST2*, with methylation percentages and coverage depths at each CpG site for each hypomethylated region indicated by pink boxes.

per beam[14,38,39]. scRNA-seq has identified a significant population of APMCs, which subsequently differentiate into more specialized APPCs[13]. Our results demonstrate that some molecular characteristics of APMCs and DPMCs resemble those of CNCCs. The *WNT1*$^{+}$ signature (*WNT1*, *SOX2*, and *HES5*) and neural plate border (*PAX3*, *PAX7*, *ZIC1*, *ZIC3*, and *TFAP2A*) genes with the exception of *MSX1* showed low expression in APMCs and DPMCs. High expression in APMCs and DPMCs was however detected in EMT/migration CNCCs signature genes (*MYC*, *ZEB2*, *ID3*, *CDH2*, *SOX9*, *MAFB*, *ID4*, *ETS1*, *EBF1*, *SNAI1*, and *CDH1*), as well as migrating/mesenchymal CNCC signatures (*MSX2*, *TWIST1*, and *PRRX2*).

The lack of expression in APMCs and DPMCs of *TFAP2A* and *SOX10*, as key regulators of the neural plate border and subsequent EMT and migration processes, is noteworthy and should be further investigated[6]. The EMT process is crucial for activating APMCs and driving antler regeneration[40], underscoring the importance of retaining these genes. *TWIST1* overexpression has been shown to induce conversion of truck NCCs to CNCCs[3], suggesting a mesenchymal CNCCs predisposition in deer APMCs. This discovery also emphasizes the deer antlerogenic periosteum as a novel embryonic reserve tissue.

This research discovered 35 core genes co-expressed between deer AP and dental pulp from adult deer and humans (Fig. 4K). We constructed a protein-protein interaction network that revealed the genes associated (Fig. 4L) with the five pluripotent stem cell regulators identified within this set (*PTN*, *GJA1*, *DLX5*, *NES*, and *FN1*). *SATB2* has previously been linked with the rejuvenation of BMSCs, and its expression decreases with aging[41]. *NOTCH2* is known to maintain stem cell pools by suppressing osteoblast differentiation[42], and *ROBO1* and *FAT3* are related via progenitor cell dynamics and self-renewal in the central nervous system[43,44]. *ROBO1* and *FAT3* expression in the adult cranial mesenchymal pools is an interesting finding. *CDH11* has been identified in CNCCs and linked to both premigratory and migratory CNCCs along with indirect modulation of Wnt/B-catenin signaling[45–47], and in addition, *DKK3* is a Wnt inhibitory factor and may be involved in the maintenance of stem cells associated with an osteogenic lineage[48]. This gene cluster represents an interconnected network present in post-embryonic CNCC-derived mesenchymal pools.

Deer antler primarily comprises bone tissue. APPCs demonstrate an exceptionally potent osteogenic capability[15,37]. Moreover, while the axial skeleton arises from mesoderm, the craniofacial periosteum originates from CNCCs, displaying a phenotype characterized by remarkable plasticity[7]. In the field of regenerative bone engineering, it is essential to consider CNCC-derived periosteal cells, such as those sourced from the palatal periosteum, as a distinctive reservoir of MCs for regenerative medicine, potentially offering superior attributes compared to those derived from the axial periosteum[49].

A consensus analysis was conducted to identify marker genes associated with CNCCs across various CNCC-derived and non-CNCC-derived MC types, offering novel insights into new markers for CNCC-derived mesenchymal pools. The gene set comprising *MSX1*, *ID3*, *CDH2*, *SOX9*, *MAFB*, *ID4*, *ETS1*, *SNAI1*, *TWIST1*, and *PRRX2* delineate CNCC and CNCC-derived mesenchymal cells within craniofacial structures (Fig. 5B), serving as crucial markers for future investigations in stem cell biology. The unique study of the CWD tusk, which has received little research attention, reveals *TFAP2A* as a marker. The expression of transcription factors *TFAP2A* and *TFAP2B* are known to be critical for determining tooth shape and defining molar versus canine shape in mice[50]; thus, they are potentially critical for the large tusk for the CWD. Intriguingly, the data clearly demonstrates that CNCC-derived MCs, whether derived from AP or tooth dental pulp tissue, exhibit high similarity and present a distinct signature compared to non-CNCC-derived tissues. These core genes associated with CNCC-derived adult mesenchymal pools lay a foundation for understanding how these pools could be leveraged in regenerative medicine.

DNA methylation plays a crucial role as an epigenetic regulator in CNCC biology[51]. Typically, DNA methylation acts to repress gene expression, representing a common epigenetic regulatory mechanism. Hypomethylation, associated with transcriptional activation during neural crest development[20], can directly lead to orofacial clefts in mice[21,52]. Our results revealed hypomethylation in the AP, correlates with early CNCC events. This suggests that epigenetic regulation via hypomethylation may establish a CNCC-derived signature, which can persist in the AP mesenchymal pools. Consequently, the DNA demethylation status emerges as a potential mechanism underlying the maintenance of multipotency in CNCC-derived adult mesenchymal pools.

Future research should prioritize validating these findings in experimental models and exploring additional regulatory mechanisms governing CNCC-derived tissue development and regeneration. Importantly, this research lays the foundation for identifying and understanding the relationship of CNCCs to their derivative mesenchymal pools and the unique attributes these cells retain for application in tissue engineering and regenerative medicine. This research has identified potential shared signature genes between mesenchymal CNCCs, AP, and teeth. We demonstrate that a 98% similarity is found between a developing MC pool in the tooth bud and APMCs, two related but spatial distinct sites, both known to have high regenerative potential. Finally, it suggests that high levels of epigenetic hypomethylation may be important in CNCCs and derivative MC pools.

Materials and methods

Tissue sampling

We collected molar dental pulp tissues from two-year-old male sika deer immediately after slaughter, following previously described procedures[53]. AP and FP tissues were obtained from one-year-old male sika deer using dissection methods outlined in our previously published paper[54]. These tissues were rapidly frozen in liquid nitrogen and stored at −80 °C for subsequent DNA extraction, facilitating whole-genome bisulfite sequencing. The animal protocol used in the present study was approved by the local animal ethics committee (Permit Number: CKARI202214).

Preparation of single-cell suspension

Fresh dental pulp tissues were carefully dissected into small pieces measuring 1 mm^3 using custom tools designed for this purpose[55]. Following the protocol for the preparation of single-cell suspension from human and mouse dental pulp[23–25], the tissue segments were digested in 10 mL Collagenase P 5 U/mL (Gibco, USA) for 120 minutes at 37 °C. The digestion process was terminated upon the release of over 50,000 cells by adding 10% (v/v) fetal bovine serum (Gibco, USA). After digestion, the cell suspensions were passed through a 70 μm filter to eliminate larger debris, and cells were collected by centrifugation at 500*g* for 5 min at 4 °C. To remove red blood cells, the cell pellets were treated with 1× red blood cell lysis buffer (Beyotime, China) for 5 min at room temperature, followed by a wash with PBS. Live cell counting was performed using an AO/PI double fluorescence staining kit (Beyotime, China).

Single-cell library construction and sequencing

Following the manufacturer's guidelines, approximately 9000–15,000 single cells were diluted and mixed with a buffer. The cell mixture was loaded into the 10× Chromium Controller, utilizing the Chromium Single Cell 3' Reagent v3 reagents. Sequencing libraries were prepared according to the manufacturer's instructions at Capitalbio Technology Corporation (Beijing, China). A 13-cycle cDNA amplification step was carried out to amplify the cDNA derived from the single cells. Subsequently, the resulting libraries were sequenced on an Illumina HiSeq 6000 platform.

Single-cell data processing

After aligning sequencing reads to a deer reference genome (NCBI: GCA_910594005.1) using Cell Ranger v6.1.2 from 10× Genomics, we conducted scRNA-seq data analysis using the R package Seurat v4.3.0[56]. To ensure high data quality, we implemented specific criteria: (1) Inclusion of cells expressing more than 200 genes; (2) retention of genes expressed in at least 3 single cells; and (3) exclusion of cells with a mitochondrial gene percentage over 8% and cells with a ribosomal gene percentage over 30%. Additionally, potential doublets were removed using the R package DoubletFinder[57] to minimize noise and artifacts. To visualize the data, we first calculated the ratio of binned variance to mean expression for each gene and selected the top 3000 most variable genes. Next, we performed principal component analysis (PCA) and reduced the data to the top 30 PCs. For integration of scRNA-seq data from different species/tissues (e.g., human, mouse, and deer), orthologous pairs were predicted using OrthoFinder v2.2.6[58] with CDS files as input. We considered only one-to-one orthologous pairs for further analysis, discarding one-to-many or many-to-many orthologous pairs. The 'Harmony' algorithm[59] was then employed to integrate the data, enhancing statistical power and mitigating batch effects. We

performed a graph-based clustering of the previously identified PCs using the Louvain Method, and the clusters were visualized on a 2D map produced with UMAP. For each cluster, we used the Wilcoxon rank-sum test to identify significantly differentially expressed genes (DEGs) when compared to the remaining clusters (Bonferroni correction was used to adjust for multiple hypothesis testing, adjusted p value < 0.01 was regarded as significant, paired tests when indicated). To visualize how well the cluster-specific DEGs (marker genes) defined each cluster, we constructed the violin plot, feature plot (UMAP plot colored by expression level of indicated genes), and heatmap (top 50 genes with highest average log-transformed fold change—logFC) using the Seurat R packages.

Cross-species cell type prediction

We utilized ScPred V1.9.2[60], which employs all principal components as gene feature space, to train the classifiers using both deer APMCs and APPCs as references. By default, prediction models use a support vector machine with a radial kernel. Subsequently, we predicted the similar probability of mouse DeMCs at various developmental stages by comparing them with the reference.

Cross-species consensus co-expression network analysis

We utilized high-dimensional WGCNA v0.2.24[61] to conduct cross-species consensus co-expression network analysis. Initially, we identified high-quality orthologous genes between deer and mouse and integrated data from APMCs, APPCs, and DeMCs. After selecting an appropriate soft power threshold, we constructed a consensus co-expression network. Module ēigengenes (MEs), which summarize the gene expression profile of entire co-expression modules, were computed for each module. Subsequently, we applied 'Harmony' batch correction to the MEs, resulting in harmonized module eigengenes (hMEs). We considered a module as a co-expression module between AP cells and DeMCs if the hME of that module exhibited high similarity between deer and mouse.

Regulon activity analysis

The transcriptional factor regulation network was predicted using SCENIC v1.1.3[62]. The co-expression module was deduced based on the Rcis Target database to construct the gene regulation module (regulon). Subsequently, the area under the curve (AUC) was calculated to indicate the regulon activity of each cell. The average regulon activity for cell types was then clustered and visualized in the heat map.

Construction of the protein–protein interaction network

The online database, STRING-db (https://string-db.org/), was employed to construct the protein-protein interaction (PPI) network, utilizing all interaction sources and setting a minimum required interaction score of ≥0.4 for our genes. Cytoscape v3.6[63] was then used to visualize the protein–protein network. Network statistics were calculated using in-house commands in Cytoscape. Key hub nodes in the network were defined based on their connective degrees with other nodes.

Gene set enrichment analysis

DAVID v2022q2[64] was used to identify gene ontology terms. We considered terms with an adjusted Fisher exact P value < 0.05.

Whole genome bisulphite sequencing and bioinformatics analysis

Briefly, two micrograms of DNA samples were initially combined with 1 ng of unmethylated lambda DNA, serving as an internal control to monitor bisulfite conversion efficiency. The DNA mixture underwent sonication using Covaris M220 to fragment the DNA into 100–300 base pair fragments. Following DNA-end repair, dA addition at the 3' end, and ligation of sequencing adaptors and index, the resulting mixtures were subjected to bisulfite conversion using the ZYMO EZ-DNA Methylation-Gold kit (Zymo Research, USA) following the standard protocol. The final libraries were sequenced on the Illumina HiSeq 6000 platform at the Beijing Genomics Institute (Wuhan, China).

Clean reads were aligned to the reference genome using Bismark v. 0.16.1[65] with default parameters. Methylcytosines were then extracted following the removal of duplicated reads. The percentage distribution and coverage depth of methylcytosines were estimated and visualized using viewBS[66]. Statistical analysis of differential methylation loci (DML) was performed utilizing the R package DSS v2.44.0[67], employing a dispersion shrinkage method for estimating the dispersion parameter from Gamma-Poisson or Beta-Binomial distributions. This method encompasses several steps: (1) estimating mean methylation levels for all CpG sites, (2) assessing dispersions at each CpG site, and (3) conducting a Wald test. Regions with multiple statistically significant CpG sites are identified as differential methylation regions (DMRs). DMRs were detected based on the results of the DML test, with a threshold for regions with difference (delta) > 0.1 and false discovery rate (FDR) < 0.05. Methylation percentages and coverage depths at each CpG site within DMRs were further visualized. Promoter regions were defined as ±1 kb around the transcription start site, and the percentage of DMRs in various genomic regions, including promoters, exons, introns, and intergenic regions, were calculated using the R package genomation v1.28.0[68].

Reporting summary

Further information on research design is available in the Nature Portfolio Reporting Summary linked to this article.

Data availability

scRNA sequencing profiling of deer dental pulp have been deposited in the OMIX, China National Center for Bioinformation/Beijing Institute of Genomics, Chinese Academy of Sciences (https://ngdc.cncb.ac.cn/omix: accession no. OMIX006856). Whole Genome Bisulfite Sequencing data of AP and FP are available in NCBI SRA (accession Nos. SRR21073940, SRR21073941, SRR21073942, and SRR21073943). Differential genome methylation regions (DMRs) between AP and FP in this study are provided as Supplementary Data 1.

Received: 7 June 2024; Accepted: 11 October 2024;
Published online: 18 October 2024

References

1. Ganesan, B. & Ramamurthy, J. Neural crest cells—ā review. *Drug Invent. Today* **11**, 768–772 (2019).
2. Shyamala, K., Yanduri, S., Girish, H. C. & Murgod, S. Neural crest: the fourth germ layer. *J. Oral. Maxillofac. Pathol.* **19**, 221–229, (2015).
3. Soldatov, R. et al. Spatiotemporal structure of cell fate decisions in murine neural crest. *Science* **364**, eaas9536 (2019).
4. Martik, M. L. & Bronner, M. E. Riding the crest to get a head: neural crest evolution in vertebrates. *Nat. Rev. Neurosci.* **22**, 616–626 (2021).
5. Pajanoja, C. et al. Maintenance of pluripotency-like signature in the entire ectoderm leads to neural crest stem cell potential. *Nat. Commun.* **14**, 5941 (2023).
6. Segundo, J. P. & Kohn, A. F. A model of excitatory synaptic interactions between pacemakers. Its reality, its generality, and the principles involved. *Biol. Cybern.* **40**, 113–126 (1981).
7. Leucht, P. et al. Embryonic origin and Hox status determine progenitor cell fate during adult bone regeneration. *Development* **135**, 2845–2854 (2008).
8. Mehrotra, P., Tseropoulos, G., Bronner, M. E. & Andreadis, S. T. Adult tissue–derived neural crest-like stem cells: sources, regulatory networks, and translational potential. *Stem Cells Transl. Med.* **9**, 328–341 (2020).
9. Pérez-Barbería, F. J. et al. What do rates of deposition of dental cementum tell us? Functional and evolutionary hypotheses in red deer. *PLoS ONE* **15**, e0231957 (2020).

10. Nakatsuka, R. et al. 5-Aza-2′-deoxycytidine treatment induces skeletal myogenic differentiation of mouse dental pulp stem cells. *Arch. Oral. Biol.* **55**, 350–357 (2010).
11. Armiñán, A. et al. Cardiac differentiation is driven by nkx2.5 and gata4 nuclear translocation in tissue-specific mesenchymal stem cells. *Stem Cells Dev.* **18**, 907–917, (2009).
12. Brandon, A. A., Almeida, D. & Powder, K. E. Neural crest cells as a source of microevolutionary variation. *Semin. Cell Dev. Biol.* **145**, 42–51 (2023).
13. Ba, H. et al. Single-cell transcriptome reveals core cell populations and androgen-RXFP2 axis involved in deer antler full regeneration. *Cell Regen. (Lond., Engl.)* **11**, 43 (2022).
14. Li, C., Yang, F. & Sheppard, A. Adult stem cells and mammalian epimorphic regeneration-insights from studying annual renewal of deer antlers. *Curr. Stem Cell Res. Ther.* **4**, 237–251 (2009).
15. Wang, D. et al. Deer antler stem cells are a novel type of cells that sustain full regeneration of a mammalian organ-deer antler. *Cell Death Dis.* **10**, 443 (2019).
16. Law, J. A. & Jacobsen, S. E. Establishing, maintaining and modifying DNA methylation patterns in plants and animals. *Nat. Rev. Genet.* **11**, 204–220 (2010).
17. Smith, Z. D. & Meissner, A. DNA methylation: roles in mammalian development. *Nat. Rev. Genet.* **14**, 204–220 (2013).
18. Jaenisch, R. & Bird, A. Epigenetic regulation of gene expression: how the genome integrates intrinsic and environmental signals. *Nat. Genet.* **33**, 245–254 (2003).
19. Cedar, H. & Bergman, Y. (Harvard Stem Cell Institute, Cambridge (MA), 2008).
20. Hu, N., Strobl-Mazzulla, P. H. & Bronner, M. E. Epigenetic regulation in neural crest development. *Dev. Biol.* **396**, 159–168 (2014).
21. Ulschmid, C. M. et al. Disruption of DNA methylation–mediated cranial neural crest proliferation and differentiation causes orofacial clefts in mice. *Proc. Natl Acad. Sci USA* https://doi.org/10.1073/pnas.2317668121 (2024).
22. De Bono, C. et al. Single-cell transcriptomics uncovers a non-autonomous Tbx1-dependent genetic program controlling cardiac neural crest cell development. *Nat. Commun.* **14**, 1551 (2023).
23. Krivanek, J. et al. Dental cell type atlas reveals stem and differentiated cell types in mouse and human teeth. *Nat. Commun.* **11**, 4816 (2020).
24. Alghadeer, A. et al. Single-cell census of human tooth development enables generation of human enamel. *Dev. Cell* **58**, 2163–2180.e2169 (2023).
25. Jing, J. et al. Spatiotemporal single-cell regulatory atlas reveals neural crest lineage diversification and cellular function during tooth morphogenesis. *Nat. Commun.* **13**, 4803 (2022).
26. Bronner, M. E. & Simões-Costa, M. in *Curr. Top. Dev. Biol*. Vol. **116** 115–134 (2016).
27. Cordero, D. R. et al. Cranial neural crest cells on the move: their roles in craniofacial development. *Am. J. Med. Genet. Part A* **155**, 270–279 (2011).
28. Li, C., Harper, A., Puddick, J., Wang, W. & McMahon, C. Proteomes and signalling pathways of antler stem cells. *PLoS ONE* **7**, e30026 (2012).
29. Allen, S. P., Maden, M. & Price, J. S. A role for retinoic acid in regulating the regeneration of deer antlers. *Dev. Biol.* **251**, 409–423 (2002).
30. Korzekwa, A. J., Kononiuk, A., Kordan, W. & Orzołek, A. Retinoic acid alters metalloproteinase action in red deer antler stem cells. *PLoS ONE* **18**, e0287782 (2023).
31. Ruan, H. et al. Sika deer antler protein against acetaminophen-induced nephrotoxicity by activating Nrf2 and inhibition FoxO1 via PI3K/Akt signaling. *Int. J. Biol. Macromol.* **141**, 961–987 (2019).
32. Bielli, A. et al. Androgen and oestrogen receptors in the growing antlers velvet of adult and yearling pampas deer (*Ozotoceros bezoarticus*) males. *doi* **50**, 947–955 (2021).
33. Mani, P., Jarrell, A., Myers, J. & Atit, R. Visualizing canonical Wnt signaling during mouse craniofacial development. *Dev. Dyn.* https://doi.org/10.1002/dvdy.22072 (2010).
34. Cao, J. et al. A human cell atlas of fetal gene expression. *Science* **370**, eaba7721 (2020).
35. Johnston, AdamP. W. et al. Dedifferentiated schwann cell precursors secreting paracrine factors are required for regeneration of the mammalian digit tip. *Cell Stem Cell* **19**, 433–448 (2016).
36. Storer, M. A. et al. Acquisition of a unique mesenchymal precursor-like blastema state underlies successful adult mammalian digit tip regeneration. *Dev. Cell* **52**, 509–524.e509 (2020).
37. Qin, T. et al. A population of stem cells with strong regenerative potential discovered in deer antlers. *Science* **379**, 840–847 (2023).
38. Landete-Castillejos, T. et al. Antlers—evolution, development, structure, composition, and biomechanics of an outstanding type of bone. *Bone* **128**, 115046 (2019).
39. Kierdorf, U., Li, C. & Price, J. S. Improbable appendages: deer antler renewal as a unique case of mammalian regeneration. *Semin. Cell Dev. Biol.* **20**, 535–542 (2009).
40. Dong, Z., Coates, D., Liu, Q., Sun, H. & Li, C. Quantitative proteomic analysis of deer antler stem cells as a model of mammalian organ regeneration. *J. Proteom.* **195**, 98–113 (2019).
41. Zhou, P. et al. SATB2-Nanog axis links age-related intrinsic changes of mesenchymal stem cells from craniofacial bone. *Aging (Milano)* **8**, 2006–2011, (2016).
42. Bai, S. et al. NOTCH1 regulates osteoclastogenesis directly in osteoclast precursors and indirectly via osteoblast lineage cells. *J. Biol. Chem.* **283**, 6509–6518 (2008).
43. Borrell, V. et al. Slit/Robo signaling modulates the proliferation of central nervous system progenitors. *Neuron* **76**, 338–352 (2012).
44. Seo, S. et al. Fat3 regulates neural progenitor cells by promoting Yap activity during spinal cord development. *Sci. Rep.* **12**, 14726 (2022).
45. Taneyhill, L. A. & Schiffmacher, A. T. Should I stay or should I go? Cadherin function and regulation in the neural crest. *Genesis* https://doi.org/10.1002/dvg.23028 (2017).
46. Chalpe, A. J., Prasad, M., Henke, A. J. & Paulson, A. F. Regulation of cadherin expression in the chicken neural crest by the Wnt/β-catenin signaling pathway. *Cell Adhes. Migr.* **4**, 431–438 (2010).
47. Sacks, D. et al. Multisociety consensus quality improvement revised consensus statement for endovascular therapy of acute ischemic stroke. *Int. J. Stroke* **13**, 612–632 (2018).
48. Byun, T. et al. Expression of secreted Wnt antagonists in gastrointestinal tissues: potential role in stem cell homeostasis. *J. Clin. Pathol.* **58**, 515–519 (2005).
49. Naung, N. Y., Duncan, W., Silva, R. D. & Coates, D. Localization and characterization of human palatal periosteum stem cells in serum-free, xeno-free medium for clinical use. *Eur. J. Oral. Sci.* **127**, 99–111 (2019).
50. Woodruff, E. D., Gutierrez, G. C., Van Otterloo, E., Williams, T. & Cohn, M. J. Anomalous incisor morphology indicates tissue-specific roles for Tfap2a and Tfap2b in tooth development. *Dev. Biol.* **472**, 67–74 (2021).
51. Yan, S., Lu, J. & Jiao, K. Epigenetic regulation of cardiac neural crest cells. *Front. Cell Dev. Biol.* https://doi.org/10.3389/fcell.2021.678954 (2021).
52. Seelan, R. S., Pisano, M. & Greene, R. M. Nucleic acid methylation and orofacial morphogenesis. *Birth Defects Res*. https://doi.org/10.1002/bdr2.1564 (2019).
53. Balic, A., Aguila, H. L., Caimano, M. J., Francone, V. P. & Mina, M. Characterization of stem and progenitor cells in the dental pulp of erupted and unerupted murine molars. *Bone* **46**, 1639–1651 (2010).
54. Li, C., Clark, D. E., Lord, E. A., Stanton, J. A. & Suttie, J. M. Sampling technique to discriminate the different tissue layers of growing antler tips for gene discovery. *Anat. Rec.* **268**, 125–130 (2002).

55. Chu, W., Zhao, H., Li, J. & Li, C. Custom-built tools for the study of deer antler biology. *Front. Biosci. (Landmark Ed.)* **22**, 1622–1633 (2017).
56. Hao, Y. et al. Integrated analysis of multimodal single-cell data. *Cell* **184**, 3573–3587.e3529 (2021).
57. McGinnis, C. S., Murrow, L. M. & Gartner, Z. J. DoubletFinder: doublet detection in single-cell RNA sequencing data using artificial nearest neighbors. *Cell Syst.* **8**, 329–337.e324 (2019).
58. Emms, D. M. & Kelly, S. OrthoFinder: solving fundamental biases in whole genome comparisons dramatically improves orthogroup inference accuracy. *Genome Biol.* **16**, 157 (2015).
59. Korsunsky, I. et al. Fast, sensitive and accurate integration of single-cell data with Harmony. *Nat. Methods* **16**, 1289–1296 (2019).
60. Alquicira-Hernandez, J., Sathe, A., Ji, H. P., Nguyen, Q. & Powell, J. E. scPred: accurate supervised method for cell-type classification from single-cell RNA-seq data. *Genome Biol.* **20**, 264 (2019).
61. Morabito, S. et al. Single-nucleus chromatin accessibility and transcriptomic characterization of Alzheimer's disease. *Nat. Genet.* **53**, 1143–1155 (2021).
62. Aibar, S. et al. SCENIC: single-cell regulatory network inference and clustering. *Nat. Methods* **14**, 1083–1086 (2017).
63. Shannon, P. et al. Cytoscape: a software environment for integrated models of biomolecular interaction networks. *Genome Res.* **13**, 2498–2504 (2003).
64. Sherman, B. T. et al. DAVID: a web server for functional enrichment analysis and functional annotation of gene lists (2021 update). *Nucleic Acids Res.* **50**, W216–221, (2022).
65. Krueger, F. & Andrews, S. R. Bismark: a flexible aligner and methylation caller for Bisulfite-Seq applications. *Bioinformatics* **27**, 1571–1572 (2011).
66. Huang, X. et al. ViewBS: a powerful toolkit for visualization of high-throughput bisulfite sequencing data. *Bioinformatics* **34**, 708–709 (2018).
67. Park, Y. & Wu, H. Differential methylation analysis for BS-seq data under general experimental design. *Bioinformatics* **32**, 1446–1453 (2016).
68. Akalin, A., Franke, V., Vlahoviček, K., Mason, C. E. & Schübeler, D. genomation: A toolkit to summarize, annotate and visualize genomic intervals. *Bioinformatics* **31**, 1127–1129 (2014).

Acknowledgements

This project was supported by the National Natural Science Foundation of China (No. U20A20403 and No. 32470892), Natural Science Foundation of Jilin Province (No. YDZJ202201ZYTS690), Jilin Province Merit Aid Study Abroad Programs (2024) and Jilin Province Development and Reform Commission (2023C040-9). The authors wish to thank Peter Fennessy of AbacusBio Limited, Dunedin, New Zealand, for reading through the manuscript and giving valuable comments.

Author contributions

C.L., D.C., and H.B. conceived and designed the research. C.M., Y.S., and Q.G. collected samples. P.H. and J.L. performed experiments. H.B. and D.C. analyzed and interpreted the data. D.C., H.B., and C.L. wrote and revised the paper. All authors have read and approved the final paper.

Competing interests

The authors declare no competing interests.

Additional information

Supplementary information The online version contains supplementary material available at https://doi.org/10.1038/s42003-024-07056-x.

Correspondence and requests for materials should be addressed to Hengxing Ba, Dawn Elizabeth Coates or Chunyi Li.

Peer review information *Communications Biology* thanks Chunmei Han, Tomas Landete-Castillejos and Maneeshi Prasad for their contribution to the peer review of this work. Primary Handling Editor: Benjamin Bessieres.